Supplement of

Global retrieval of TROPOMI tropospheric HCHO and NO_2 columns with improved consistency based on updated Peking University OMI NO_2 algorithm

Yuhang Zhang et al.

Correspondence to: Jintai Lin (linjt@pku.edu.cn) , Michel Van Roozendael (michel.vanroozendael@aeronomie.be)

Table S1. Specifics for the HCHO and NO_2 SCD retrieval of TROPOMI operational products.

Parameter	HCHO (v2.4.1)	NO_2 (v2.4.0)
Type of DOAS fit	Optical fit	Intensity fit
Fitting interval	328.5-359 nm	405-465 nm
Absorption cross sections	HCHO, Meller and Moortgat (2000), 298 K	NO_2, Vandaele et al. (1998), 220 K
	NO_2, Vandaele et al., (1998), 220 K	O_3, Serdyuchenko et al. (2014), 243 K
	O_3, Serdyuchenko et al. (2014), 223 + 243 K	O_2-O_2, Thalman and Volkamer (2013), 293 K
	BrO, Fleischmann et al. (2004), 223 K	H_2O_{vap} based on HITRAN 2012 data (van
	O_2-O_2, Thalman and Volkamer (2013), 293 K	Geffen et al., 2015)
	Ring effect, Chance and Spurr (1997)	H_2O_{liq}, Pope and Fry (1997)
	Non-linear O_3 absorption effect, Puķīte et al. (2010)	Ring effect, Chance and Spurr (1997)
Slit function	Pre Flight Model	Pre Flight Model
Polynomial	5^{th} order	5^{th} order
Intensity offset correction	Linear offset	Currently turned off
Reference spectrum I_0	Average of radiances, per row, selected in the equatorial Pacific within the last 5 valid days	High-resolution solar reference spectrum, Chance and Kurucz (2010)

Table S2. Statistics of separate validation results against ground-based MAX-DOAS and PGN measurements.

HCHO	MAX-DOAS		PGN	
	POMINO	RPRO	POMINO	RPRO
Slope	0.54	0.62	0.57	0.61
Offset [10^{15} molec.cm^{-2}]	2.19	0.37	0.79	0.22
Correlation	0.68	0.70	0.61	0.66
NMB	−26.3%	−32.3%	−31.7%	−35.6%
NO_2	MAX-DOAS		PGN	
	POMINO	RPRO	POMINO	RPRO
Slope	0.65	0.58	0.77	0.69
Offset [10^{15} molec.cm^{-2}]	0.77	0.70	0.70	0.81
Correlation	0.83	0.85	0.84	0.86
NMB	−17.5%	−27.8%	−5.3%	−14.9%

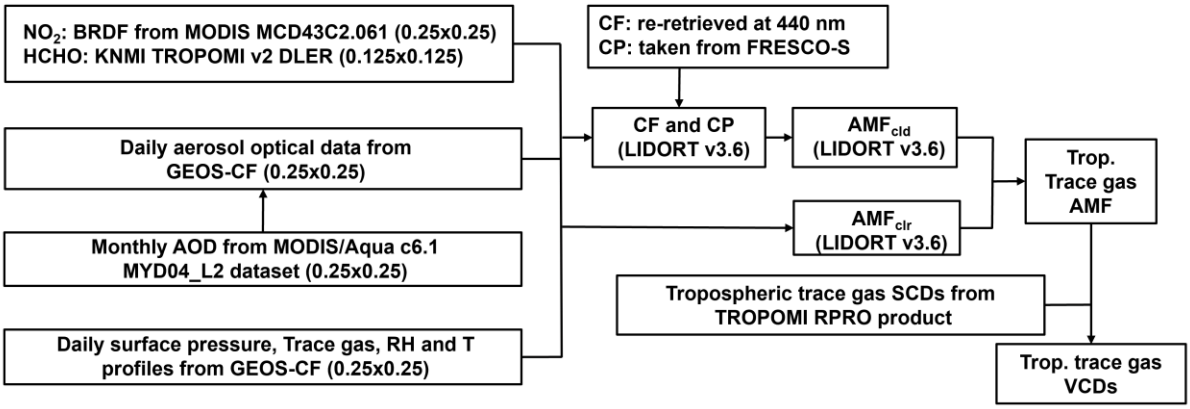

Figure S1. Flow chart of global POMINO-TROPOMI algorithm for consistent HCHO and NO_2 AMF calculation.

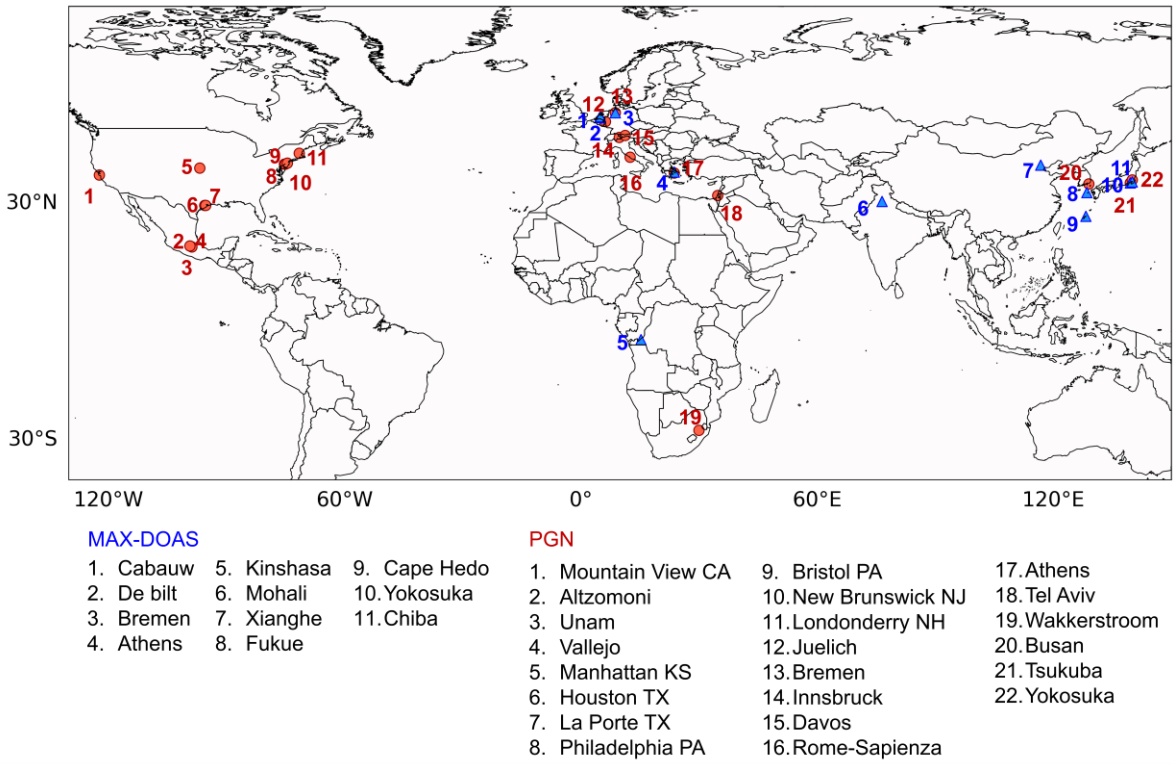

Figure S2. Spatial distribution of ground-based MAX-DOAS and PGN sites selected for validation in this study.

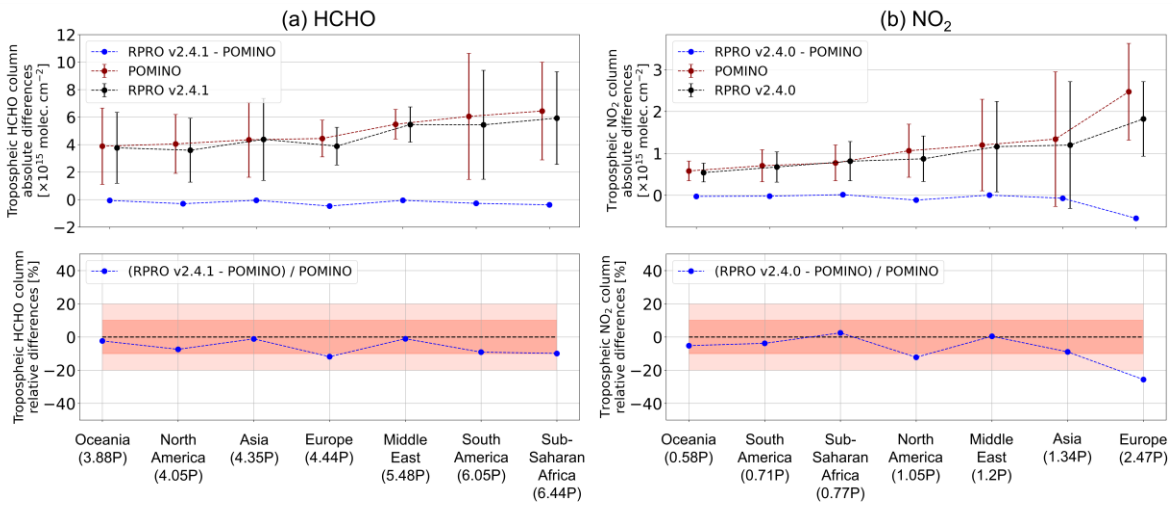

Figure S3. Absolute and relative differences between POMINO and RPRO (**a**) HCHO and (**b**) NO_2 tropospheric columns averaged in April, July, October 2021, and January 2022 in seven regions. Regions are sorted as a function of POMINO mean HCHO or NO_2 columns, with values (in the unit of "P" as Pmolec.cm^{-2} = 1 × 10^{15} molec.cm^{-2}) shown in the brackets in the bottom axis. Mean POMINO (red) and RPRO (black) columns are also plotted with the absolute differences in the upper panel. Error bars represent the standard deviations of the columns. Pink areas indicate 10% and 20% relative differences.

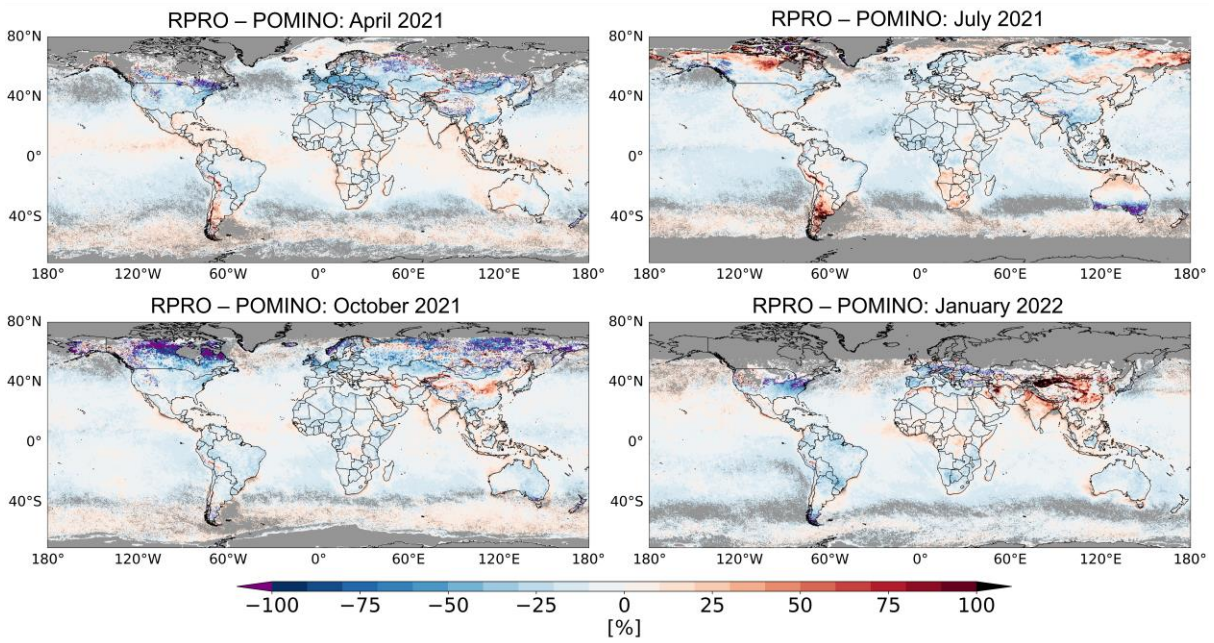

Figure S4. Relative differences of tropospheric HCHO columns of RPRO to POMINO in April 2021, July, October 2021 and January 2022. The regions in gray mean that there are no valid observations.

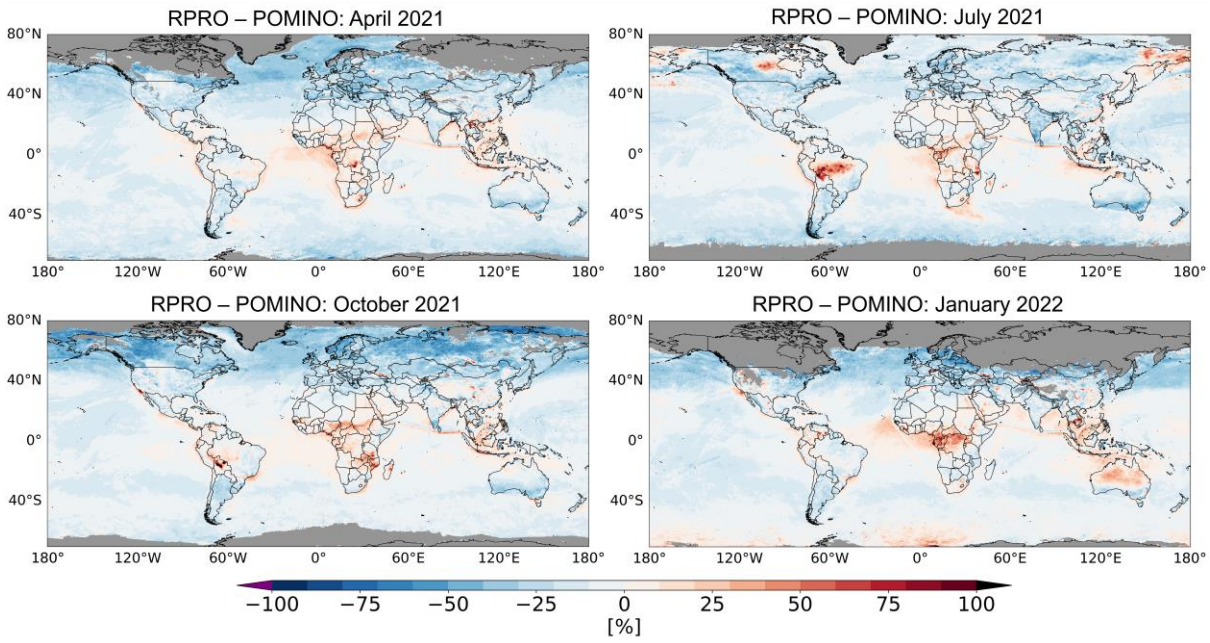

Figure S5. Similar to Figure S4 but for NO_2.

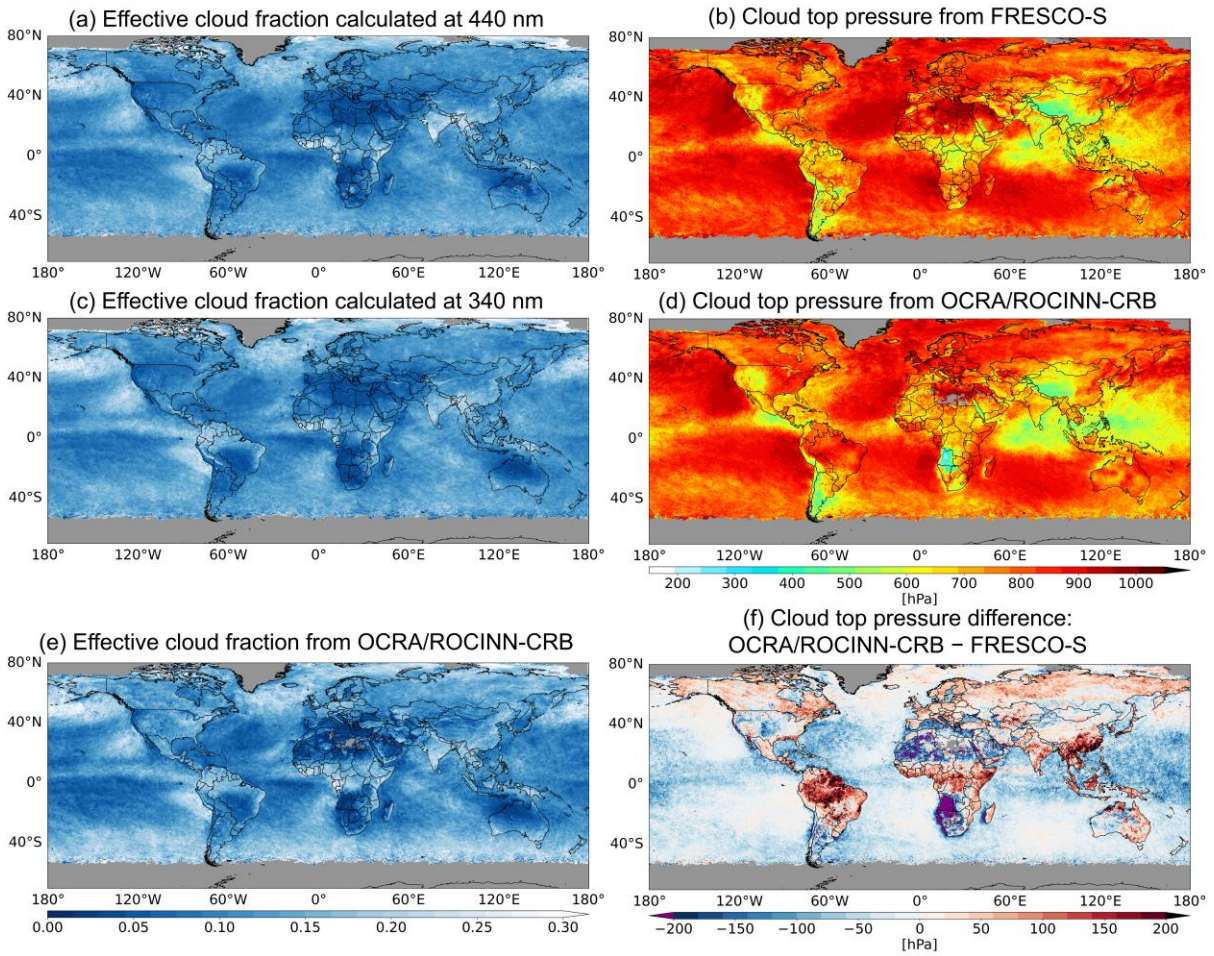

Figure S6. Comparison of cloud parameters used for sensitivity tests in July 2021. (**a**) POMINO-based effective cloud fraction calculated at 440 nm; (**b**) cloud top pressure from FRESCO-S product; (**c**) POMINO-based effective cloud fraction calculated at 340 nm; (**d**) cloud top pressure from OCRA/ROCINN-CRB product; (**e**) effective cloud fraction from OCRA/ROCINN-CRB product and (**f**) difference of (**d**) to (**b**). Pixels with HCHO QA > 0.5 and ECF of each case > 0.01 are included. The regions in gray mean that there are no valid observations.

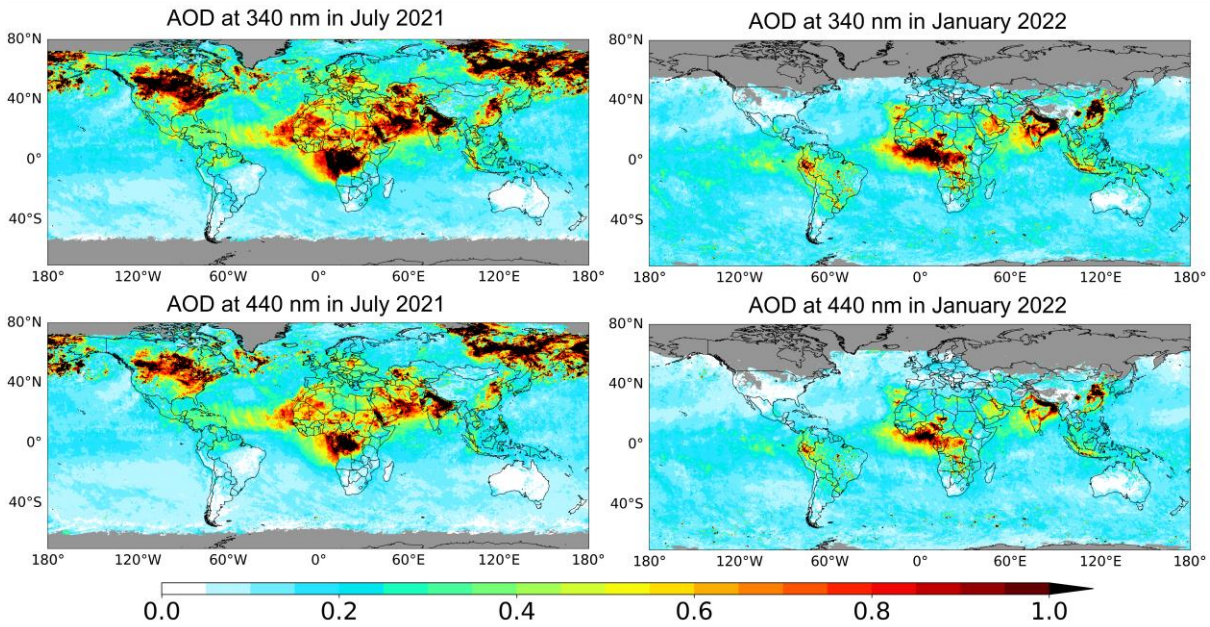

Figure S7. Spatial distribution of monthly AOD in July 2021 and January 2022 used in POMINO retrieval at 340 nm (first row) and 440 nm (second row). The regions in gray mean that there are no valid TROPOMI observations.

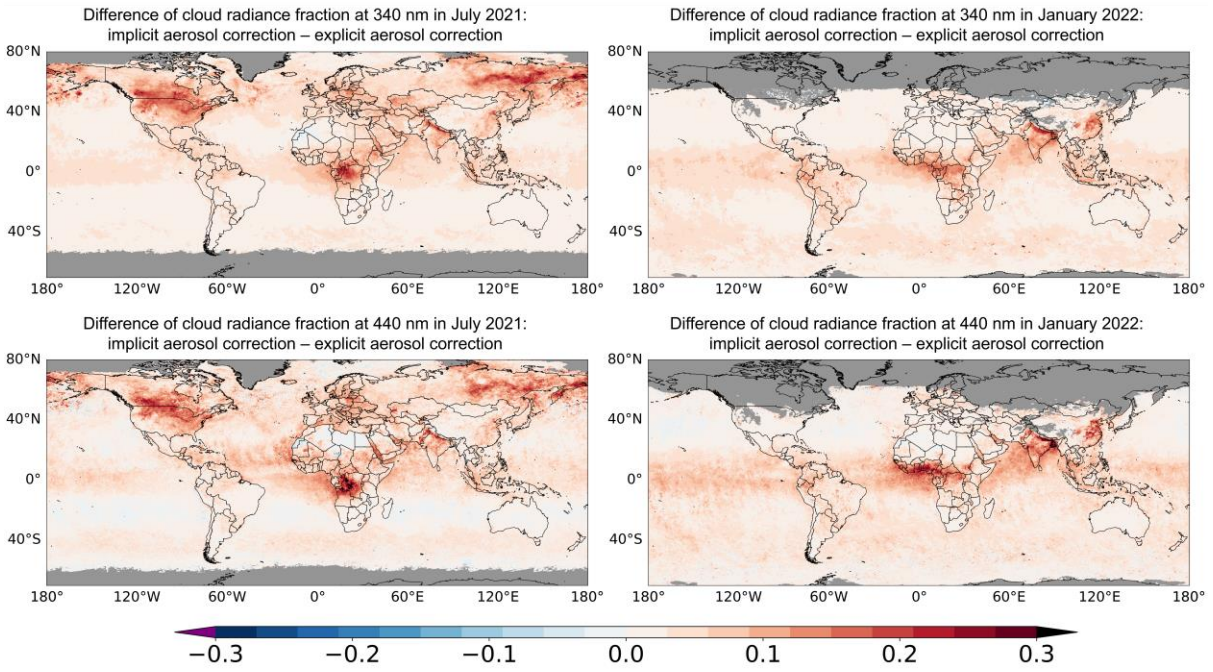

Figure S8. Absolute differences of cloud radiance fractions retrieved with implicit aerosol corrections (Cases "Fst_imaer" and "Nst_imaer") to those with explicit aerosol corrections (Case "Fst_ORcp" and POMINO NO_2) in July 2021 and January 2022 at 340 nm (first row) and 440 nm (440 nm). The regions in gray mean that there are no valid observations.

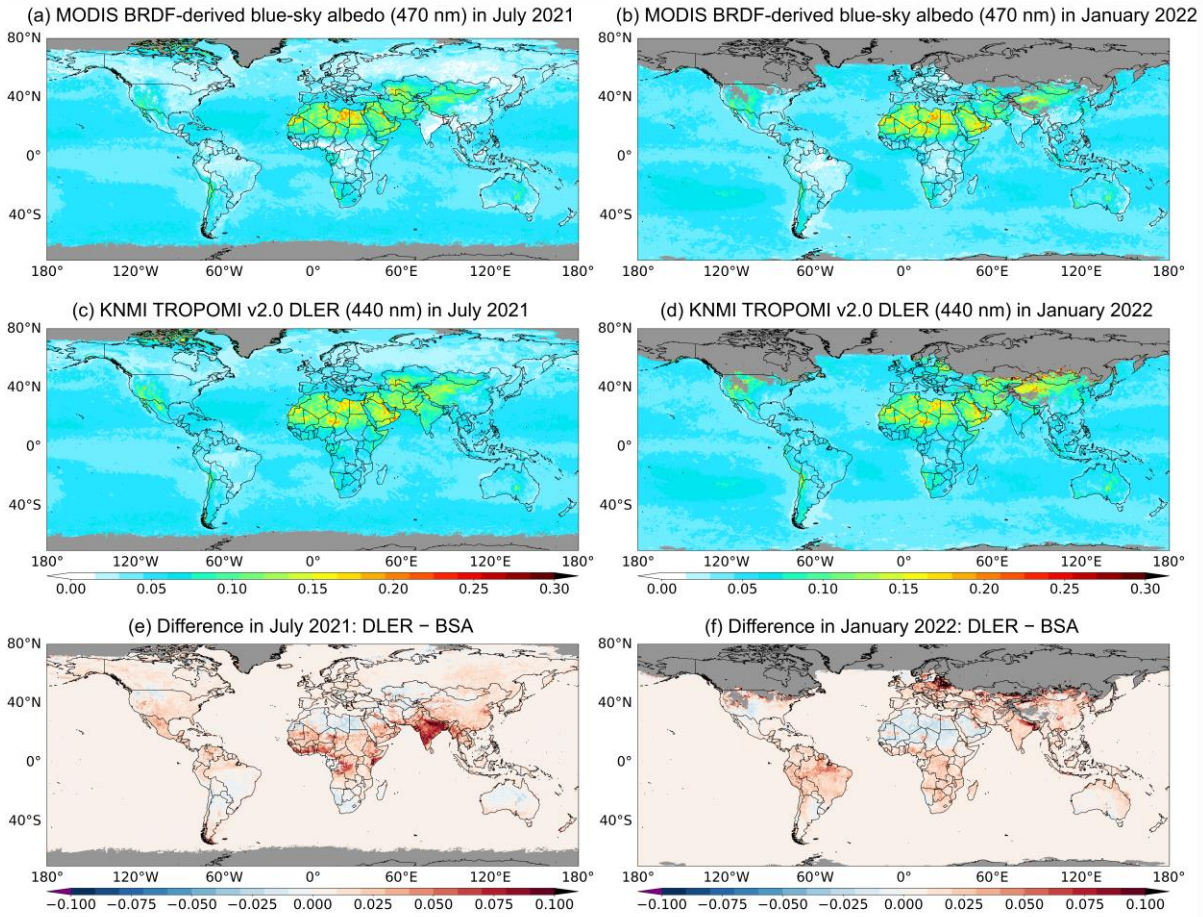

Figure S9. Spatial distribution of MODIS BRDF-derived blue-sky albedo (**a** and **b**), KNMI TROPOMI v2.0 DLER at 440 nm (**c** and **d**), and their absolute differences (**e** and **f**) in July 2021 and January 2022. The regions in gray mean that there are no valid observations.

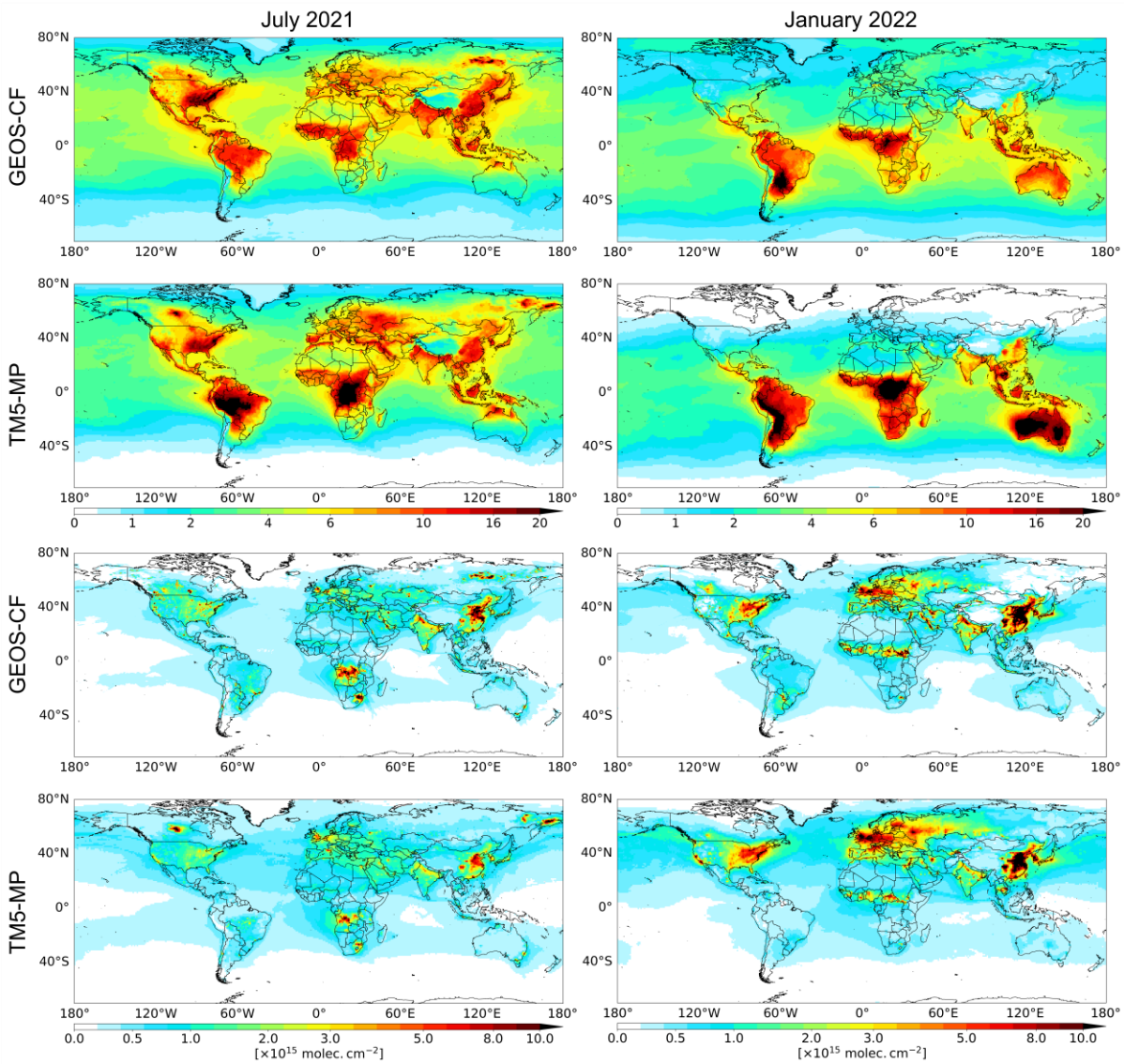

Figure S10. Spatial distribution of GEOS-CF and TM5-MP tropospheric HCHO (first and second rows) and NO_2 (third and fourth rows) VCDs in July 2021 and January 2022.

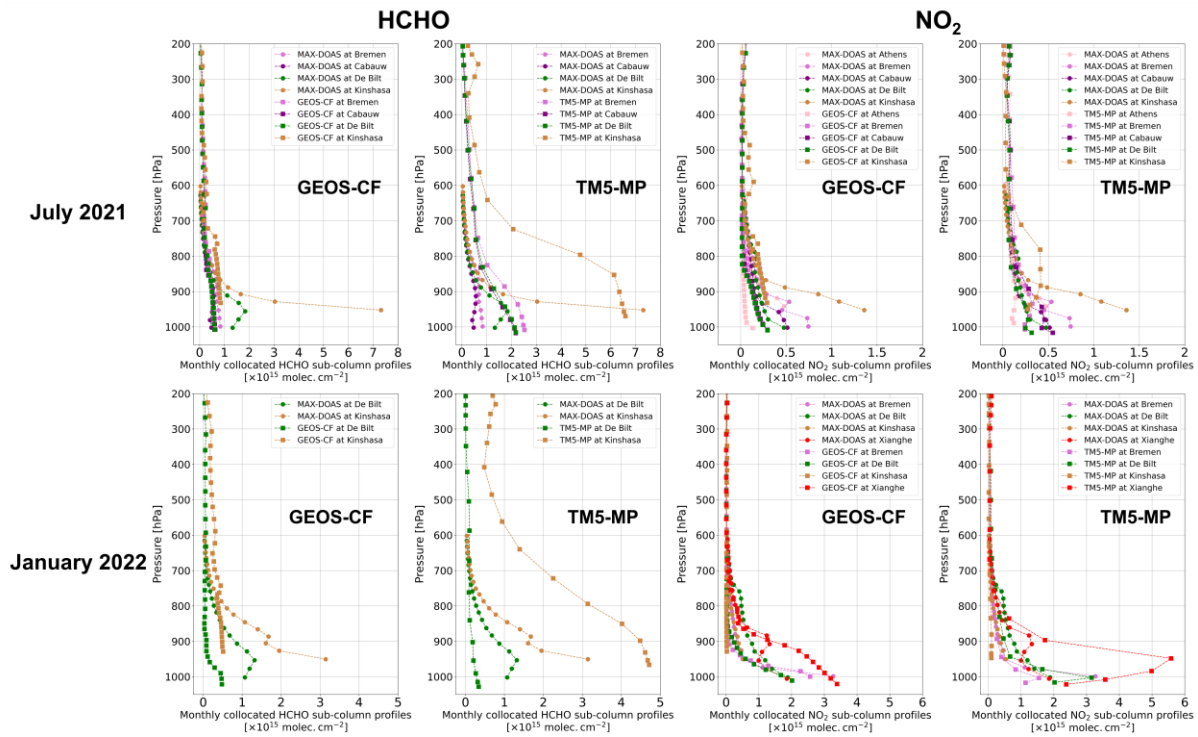

Figure S11. Comparisons of monthly collocated HCHO and NO_2 sub-column profiles between models (GEOS-CF or TM5-MP) and ground-based MAX-DOAS measurements in July 2021 and January 2022.

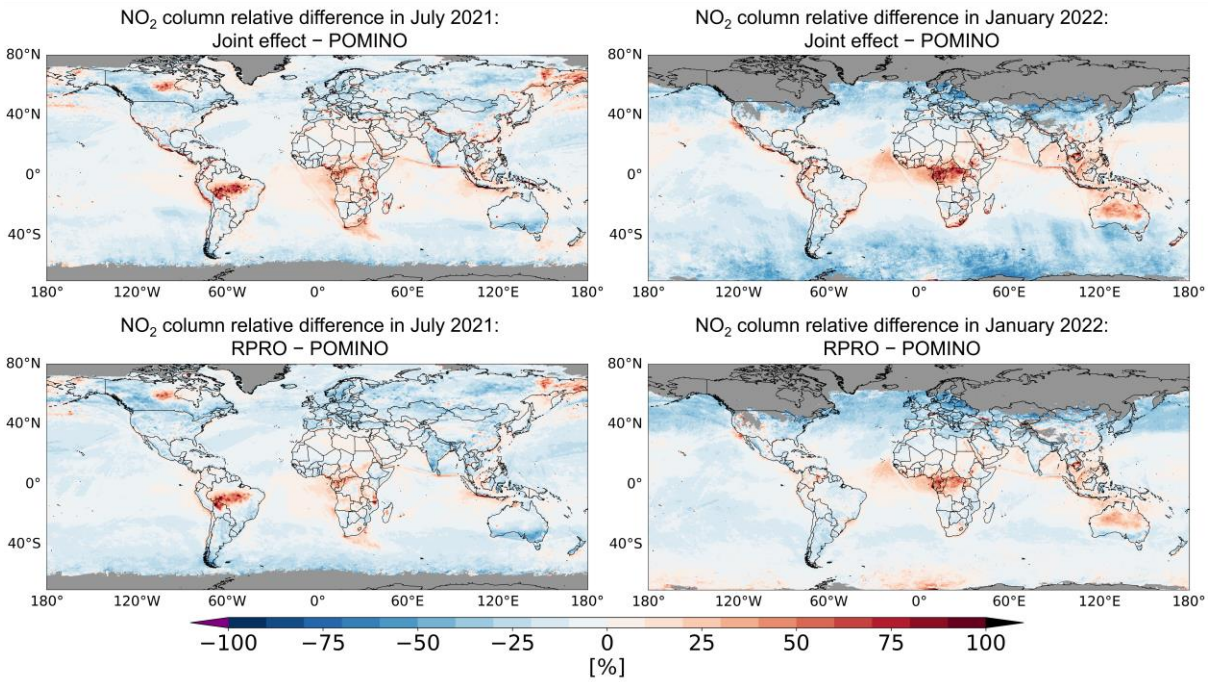

Figure S12. Relative differences of tropospheric NO_2 columns of sensitivity test "Nst_joint" (Case N4) to POMINO (first row) and those of RPRO to POMINO (second row) in July 2021 and January 2022. The regions in gray mean that there are no valid observations.

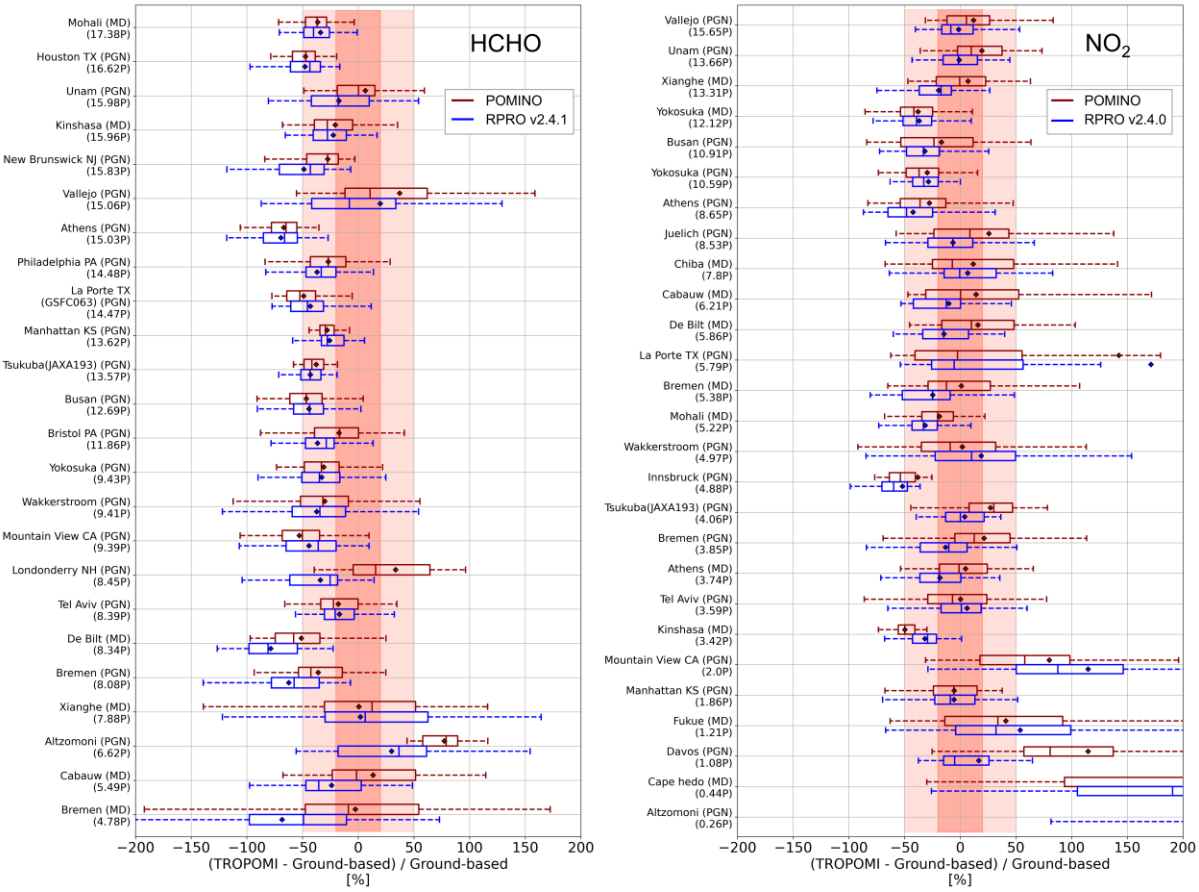

Figure S13. Box-and-whisker plots for the bias and spread of the relative difference of tropospheric HCHO (left) and NO_2 (right) columns between TROPOMI products (POMINO in red and RPRO in blue) and ground-based measurements. The box extends from the first quartile to the third quartile of the data, and the vertical solid line inside it represents the median difference. Mean difference is also shown by the diamond mark, and the whiskers extend from the box to the farthest data point lying within 1.5 times the inter-quartile range (IQR) from the box. The sites are ordered as a function of mean ground-based tropospheric columns in April, July, October 2021, and January 2022 (shown in the brackets in the unit of "P" as Pmolec.cm^{-2} = 1 × 10^{15} molec.cm^{-2}). "MD" represents MAX-DOAS sites and "PGN" represents PGN sites.

References

Chance, K. and Kurucz, R. L.: An improved high-resolution solar reference spectrum for earth's atmosphere measurements in the ultraviolet, visible, and near infrared, Journal of Quantitative Spectroscopy and Radiative Transfer, 111, 1289–1295, https://doi.org/10.1016/j.jqsrt.2010.01.036, 2010.

Chance, K. V. and Spurr, R. J. D.: Ring effect studies: Rayleigh scattering, including molecular parameters for rotational Raman scattering, and the Fraunhofer spectrum, Appl. Opt., AO, 36, 5224–5230, https://doi.org/10.1364/AO.36.005224, 1997.

Fleischmann, O. C., Hartmann, M., Burrows, J. P., and Orphal, J.: New ultraviolet absorption cross-sections of BrO at atmospheric temperatures measured by time-windowing Fourier transform spectroscopy, Journal of Photochemistry and Photobiology A: Chemistry, 168, 117–132, https://doi.org/10.1016/j.jphotochem.2004.03.026, 2004.

van Geffen, J. H. G. M., Boersma, K. F., Van Roozendael, M., Hendrick, F., Mahieu, E., De Smedt, I., Sneep, M., and Veefkind, J. P.: Improved spectral fitting of nitrogen dioxide from OMI in the 405–465 nm window, Atmospheric Measurement Techniques, 8, 1685–1699, https://doi.org/10.5194/amt-8-1685-2015, 2015.

Meller, R. and Moortgat, G. K.: Temperature dependence of the absorption cross sections of formaldehyde between 223 and 323 K in the wavelength range 225–375 nm, Journal of Geophysical Research: Atmospheres, 105, 7089–7101, https://doi.org/10.1029/1999JD901074, 2000.

Pope, R. M. and Fry, E. S.: Absorption spectrum (380–700 nm) of pure water. II. Integrating cavity measurements, Appl. Opt., AO, 36, 8710–8723, https://doi.org/10.1364/AO.36.008710, 1997.

Puķīte, J., Kühl, S., Deutschmann, T., Platt, U., and Wagner, T.: Extending differential optical absorption spectroscopy for limb measurements in the UV, Atmospheric Measurement Techniques, 3, 631–653, https://doi.org/10.5194/amt-3-631-2010, 2010.

Serdyuchenko, A., Gorshelev, V., Weber, M., Chehade, W., and Burrows, J. P.: High spectral resolution ozone absorption cross-sections – Part 2: Temperature dependence, Atmospheric Measurement Techniques, 7, 625–636, https://doi.org/10.5194/amt-7-625-2014, 2014.

Thalman, R. and Volkamer, R.: Temperature dependent absorption cross-sections of O2–O2 collision pairs between 340 and 630 nm and at atmospherically relevant pressure, Phys. Chem. Chem. Phys., 15, 15371–15381, https://doi.org/10.1039/C3CP50968K, 2013.

Vandaele, A. C., Hermans, C., Simon, P. C., Carleer, M., Colin, R., Fally, S., Mérienne, M. F., Jenouvrier, A., and Coquart, B.: Measurements of the NO2 absorption cross-section from 42 000 cm−1 to 10 000 cm−1 (238–1000 nm) at 220 K and 294 K, Journal of Quantitative Spectroscopy and Radiative Transfer, 59, 171–184, https://doi.org/10.1016/S0022-4073(97)00168-4, 1998.